J Mol Model (2010) 16:929–938
DOI 10.1007/s00894-009-0599-6

ORIGINAL PAPER

Insight into the interaction sites between fatty acid binding proteins and their ligands

Lihie Ben-Avraham Levin · Assaf Ganoth · Shay Amram · Esther Nachliel · Menachem Gutman · Yossi Tsfadia

Received: 1 July 2009 / Accepted: 20 September 2009 / Published online: 16 October 2009

Abstract Fatty acid binding proteins (FABPs), are evolutionarily conserved small cytoplasmic proteins that occur in many tissue-specific types. One of their primary functions is to facilitate the clearance of the cytoplasmic matrix from free fatty acids and of other detergent-like compounds. Crystallographic studies of FABP proteins have revealed a well defined binding site located deep inside their β-clam structure that is hardly exposed to the bulk solution. However, NMR measurements revealed that, when the protein is equilibrated with its ligands, residues that are clearly located on the outer surface of the protein do interact with the ligand. To clarify this apparent contradiction we applied molecular dynamics simulations to follow the initial steps associated with the FABP–fatty acid interaction using, as a model, the interaction of toad liver basic FABP, or chicken liver bile acid binding protein, with a physiological concentration of palmitate ions. The simulations (~200 ns of accumulated time) show that fatty acid molecules interact, unevenly, with various loci on the protein surface, with the favored regions being the portal and the anti-portal domains. Random encounters with palmitate at these regions led to lasting adsorption to the surface, while encounters at the outer surface of the β-clam were transient. Therefore, we suggest that the protein surface is capable of sequestering free fatty acids from solution, where brief encounters evolve into adsorbed states, which later mature by migration of the ligand into a more specific binding site.

Keywords Fatty acid · Fatty acid binding protein · Molecular dynamics simulation · Protein–ligand interaction

L. Ben Avraham Levin and A. Ganoth contributed equally to this work.

Electronic supplementary material The online version of this article (doi:10.1007/s00894-009-0599-6) contains supplementary material, which is available to authorized users.

L. B.-A. Levin · A. Ganoth · S. Amram · E. Nachliel · Y. Tsfadia (✉)
Department of Biochemistry,
George S. Wise Faculty of Life Sciences, Tel Aviv University,
Tel Aviv, Israel
e-mail: yossit@tauex.tau.ac.il

E. Nachliel · M. Gutman
Laser Laboratory for Fast Reactions in Biology,
Department of Biochemistry, George S. Wise
Faculty of Life Sciences, Tel Aviv University,
Tel Aviv, Israel

Present Address:
A. Ganoth
Department of Biological Chemistry, Institute of Life Sciences,
The Hebrew University,
Jerusalem, Israel

Abbreviations

FA	Fatty acid
FABP	Fatty acid binding protein
Lb-FABP	Liver basic FABP
L-BABP	Liver bile acid binding protein
LJ	Lennard-Jones
MD	Molecular dynamics
PB	Poisson-Boltzmann
PDB	Protein data bank
PLM	Palmitate
PME	Particle mesh Ewald
RMSD	Root mean square deviation
SASA	Solvent accessible surface area
SPC	Simple point charge
VdW	Van der Waals
VMD	Visual MD

Introduction

Fatty acids (FAs) serve as a major energy source and as a structural element of phospholipid membranes. Due to their detergent-like properties, the concentration of free FA needs to be suppressed. For this reason, the transfer of free FA in the brush border cells, from the cell membrane facing the gut lumen to the ER, is mediated by members of the fatty acid binding protein (FABP) family.

Mammalian FABPs were discovered in the early 1970s as abundant cytoplasmic proteins, and found to be tissue-specific. Very high sequence conservation has been shown to exist between FABPs isolated from the same tissue in different species [1–5], whereas the different FABP types in one species show amino acid sequence identities ranging from 20% to 70% [3–7]. The FABPs share a common structure: ten β-strands, forming a β-clam configuration that encloses an inner space covered by two α-helices. Two β-strands, named D and E, flank the portal domain—an expandable gap through which the FA molecule can squeeze in and penetrate into an inner binding pocket [8, 9]. The two α-helices that cap the portal domain have been shown to function as a membrane-high-affinity site [8, 10–15]. The complex mode of FAs and other lipid compounds (like cholesterol, retinoic acid, mono-glycerides) have been studied intensively by crystallographic methods [11, 16–18]. In all cases, the ligand was embedded inside the β-clam structure, either as a single molecule, or as a pair of ligands (in the liver type FABP proteins). Unlike most enzymes, where the substrate binding site is well exposed to the bulk solution, the FABP protein sequesters the ligand inside a well secured cavity into which the FA must squeeze itself. This is a complex process that calls for repeated conformational changes, where the FA and the protein adopt their structures to fit each other. Consequently, it is fascinating to follow the dynamics of the interaction of the FABP and its ligand.

Of special interest are the recent observations of Scanlon and co-workers [19, 20], who noted that, even at sub-millimolar concentrations of ligands [like oleate, Aniline-Naphtalen-Sulfonate (ANS), progesterone or various drugs], the ligand interacts with the protein over a large area of its surface, including residues located on the outer surface of the α-helix regions that make no contact with the inner space of the ligand binding cavity. This observation suggests that transient ligand adsorption events take place all over the surface of the protein, some of them lasting enough to be detected as part of the population of states sampled by the NMR detectable interactions. Thus, the formation of the stable complex as envisioned by X-ray is probably a product of a gradual process having a temporal periodical element that leaves no marks on the final crystalline state of the protein.

Various computational studies have been conducted to follow the dynamics of FABPs, either in the presence of a ligand or in its absence. Yet, to the best of our knowledge, the possibility that there is no single major exclusive interaction site has not been fully explored [21–37]. Our previous molecular dynamics (MD) simulations first illustrated the interaction of FA with the portal and the anti-portal domains of the protein [23, 24, 37]. In the present publication, we report the outcome of a comprehensive simulative effort (accumulated to ~200 ns), carried out with non-mammalian (toad and chicken) Lb-FABP (also known as L-BABP) proteins, looking at the general features of their interaction with the same molecule: palmitate (PLM). The simulations, carried out under ionic strength and ligand concentrations resembling physiological conditions, were initiated with an *Apo*-protein and few PLM anions. The dynamics were followed over time until the root mean square deviation (RMSD) of the protein's α-carbon atoms attained a relatively stable value. It should be noted that the limited time interval that can be simulated is in the range of a few tens of nanoseconds—too short to yield a structure comparable with either the configuration imposed by crystallization conditions or the well equilibrated solution used for NMR measurement. Thus, the generated structure reflect initial pre-equilibrium states that the experimental structural methods are blind to, structures that until now have not been studied. Multiple interactions were visualized through analyzing the various sites of interaction, and scored by the stability of the encounter complex and the spatial distribution of the more stable complexes.

The results imply that the initial interaction of the FA with the protein is seemingly a random diffusion controlled event, followed by a preferred adherence of the FA to the portal and the anti-portal domains, representing the degeneracy of the transient encounter complexes. This spread of contact area is in accord with the results of NMR measurements. Based on the diversity of the complex structures, we were able to assign some 'sponge'-like characteristics to the initial interactions of the protein with the FA molecules: the protein first sequesters the cytoplasmic space from the mild-detergent function of the ionized free FAs (pK_a=4.8 [38]), which are capable of disrupting sensitive intra-cellular structures.

Materials and methods

Molecular dynamics simulations

The MD simulations were performed using the GROMACS 3.3.1 package of programs [39–41], with the GROMOS96 53A6 force field [42]. The coordinates for toad (PDB code

1P6P) and chicken (PDB code 1TVQ) Lb-FABP, determined by X-ray crystallography at 2.5 Å [6] and 2.0 Å [7], respectively, were downloaded from the Protein Data Bank (PDB) [43]. The lipid topology files, as needed in GROMACS, were prepared using the PRODRG server [44]. The protein and the ligand were embedded in a truncated octahedral box containing about 10,000 water molecules using the SPC water model [45] that extended to 12–15 Å between the protein and the edge of the box.

A total of 11 simulations were performed, either with toad or chicken Lb-FABP. Each simulation had a different initial location of the PLM molecules, initial velocities and number of PLM ions present in the reaction system (see Table S1). The PLM molecules were placed randomly within the simulation box, but special care was taken to ensure that the initial position of the PLM molecules was outside the protein structure. Assuming normal charge states of dissociable groups corresponding to pH 7, the net charge of the toad Lb-FABP is Z=0, and that of the chicken L-BABP is Z=+2e. The negative charge on the proteins, as well as that of the PLM anion, was neutralized by the addition of Na^+ ions. Besides these ions, more Na^+ and Cl^- ions were added to maintain the ionic strength of the solution within the range 50–100 mM (see Table S1). Prior to MD simulations, internal constraints were relaxed by energy minimization. Following minimization, 100 ps equilibration runs were performed under position restraints of the carbon backbone atoms through a harmonic force constant of 1,000 kJ mol^{-1} nm^{-2} followed by unrestrained MD simulations. The first 100 ps of the runs were treated as a further equilibration, and the remainder were saved and used for the analysis. During the MD runs, the LINCS algorithm [46] was used to constrain the lengths of all bonds; the water molecules were restrained using the SETTLE algorithm [47]. The time step for the simulations was 2 fs. The simulations were run under NPT conditions, using Berendsen's coupling algorithm for keeping the temperature and the pressure constant (P=1 bar; τ_P= 0.5 ps; τ_T=0.1 ps; T=300 K) [48]. Van der Waals (VdW) forces were treated using a cutoff of 12 Å. Long-range electrostatic potentials were treated using the Particle mesh Ewald (PME) method [49]. The coordinates were saved every 1 ps.

Visual presentations

All protein figures were created using the Visual Molecular Dynamics (VMD) computer program [50].

Lennard-Jones interactions

Lennard-Jones (LJ) interactions were computed using a standard GROMACS utility.

Electrostatic interactions

Short-range electrostatic interactions were computed using a standard GROMACS utility with cutoff of 12 Å. To verify that the calculations were also valid for longer ranges, they were repeated with cutoffs of 14, 16, 18, and 20 Å. As expected, longer ranges did not affect the trend of the results.

Results and discussion

Molecular dynamics simulations of Lb-FABP with PLM molecules

MD simulations were carried out in an explicit water model and at 50–100 mM NaCl in the presence of 3 or 4 molecules of PLM. The outcome of a typical three simulations, in the form of RMSD of the α-carbons, is presented in Fig. 1. The protein seemed to be fairly stable throughout the simulations, with mild fluctuations up to 0.2–0.25 nm. The PLM molecules, while binding mainly to the portal and anti-portal domains, twice formed a mini micelle that migrated to the anti-portal. There were no significant differences in the RMSD of the protein between simulations where the PLM molecules interact at the portal region, and simulations in which a mini micelle attached to its anti-portal domain. The β-barrel arrangement of the protein creates a stable rigid structure with very few flexible regions. Simulations of the same system, where the initial locations of the PLM molecules and the initial velocities varied, were repeated 11 times covering ~200 ns simulation time. Examination of the trajectories of the simulations listed in Table S1 indicates that encounters of the small molecules with the protein take place all over the surface of the protein, yet mainly with its portal and anti-portal regions. Some of the encounters were brief, lasting only a few picoseconds, while others appeared to be more stable. As the simulations progressed, both the structure of the protein and the FA molecules reached relatively stable configurations, which changed little as the simulation time approached 20 ns. These configurations may evolve much later into the well equilibrated states observed in NMR experiments. Representative snapshots, taken when the simulations were terminated, are presented in Fig. 2.

Generally, we identified the following reacting domains: the two α-helices that form the lid over the inner cavity; the portal domain, which is the slit between the D and E β-strands and the lid on top of it; the outer surface of the β-clam barrel; and the anti-portal region located at the junction of the turn structures that link the β-strands at the bottom of the barrel (see Fig. 2f for definition of the

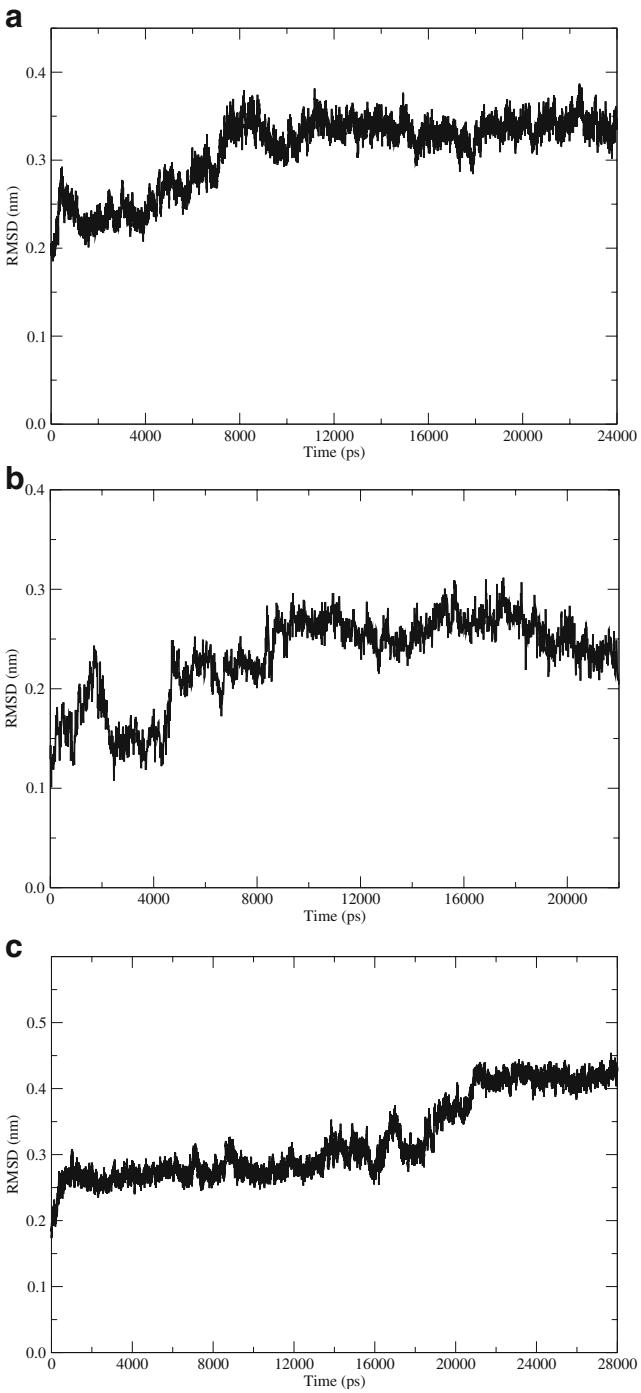

Fig. 1a–c Root mean square deviation (RMSD) of the liver basic fatty acid binding protein (Lb-FABP) from toad. **a** and **b** represent simulations P6P_VI and P6P_V, respectively (see Table S1). In these simulations, palmitate (PLM) molecules penetrated and adsorbed to the main portal region. **c** A simulation where a mini micelle interacted with the anti-portal domain (P6P_VII)

reactive domains). All these regions, except for the outer surface of the β-clam, were found to be associated with PLM molecules that remained in contact for an appreciable period, extending the few picoseconds of an accidental encounter. Figure 2a shows the FA molecule bound to the outer surface of the α-helices domain, causing a partial unfolding of the α-helix. In Fig. 2b, one PLM molecule is perched on the portal domain, well under the two α-helices lid, while in Fig. 2c we find two FA molecules located under the lid at the portal domain. The other attractive domain for PLM molecules is the anti-portal section, located at the junction of the turn-loops that connect the β strands, where the PLM molecule can either fit in with its carboxylate moiety inserted inside the protein (Fig. 2d), or for attachment of a mini-micelle (Fig. 2e).

It is of interest to point out that the outer structure of the β-clam, making the most of the protein's surface, appeared to have the lowest affinity for PLM adsorption. Out of the ~200 ns simulation time, only a few occasional contacts were made between the ligand and the outer surface of the β-clam area of the protein. Thus, size does not matter when one looks for adsorption events. This lack of lasting contact with the β-clam makes it interesting to look at the energetic profiles involved in the transformation of a random encounter between the FA and the protein into a complex with a lifetime of more than a fraction of a nanosecond.

Energy determinants affecting adsorption of FA to the protein

Figure 3 depicts the time evolution of the electrostatic and LJ potentials as calculated for the protein–PLM interactions during the simulation time. In all cases, both potentials were zero at the time of initiation, indicating that the reaction was not affected by the initial location of the FA. With time, both potentials had decreased as the PLM and the protein made contact. The traces presented in the figure are typical examples. Figure 3a corresponds to the interaction of a single FA molecule with the helices that cap the portal region (see also Fig. 2a); Fig. 3b represents the interaction of a single FA in the portal domain (Fig. 2b); Fig. 3c depicts the variation of the potentials as two FA molecules interact with the portal domain (Fig. 2c). In this case, the total LJ potential reaches a value of ~ (−180) kJ mol^{-1}, where in cases where only one PLM ion is bound, the value is close to −100 kJ mol^{-1}. Figure 3d,e record the binding of one or three PLM molecules to the anti-portal domain (corresponds to Fig. 2d,e).

The interaction energies presented in Fig. 3 share some common features, although each corresponds to a singular simulation of the system. In all simulations, the component dominating the potential energy is the LJ attraction energy, which appears as a time stable potential with a magnitude ~100 kJ mol^{-1}. The electrostatic potential behaves in a more erratic mode, fluctuating between 0 (sometimes even repulsive) and ~ (−200) kJ mol^{-1}, and is associated with

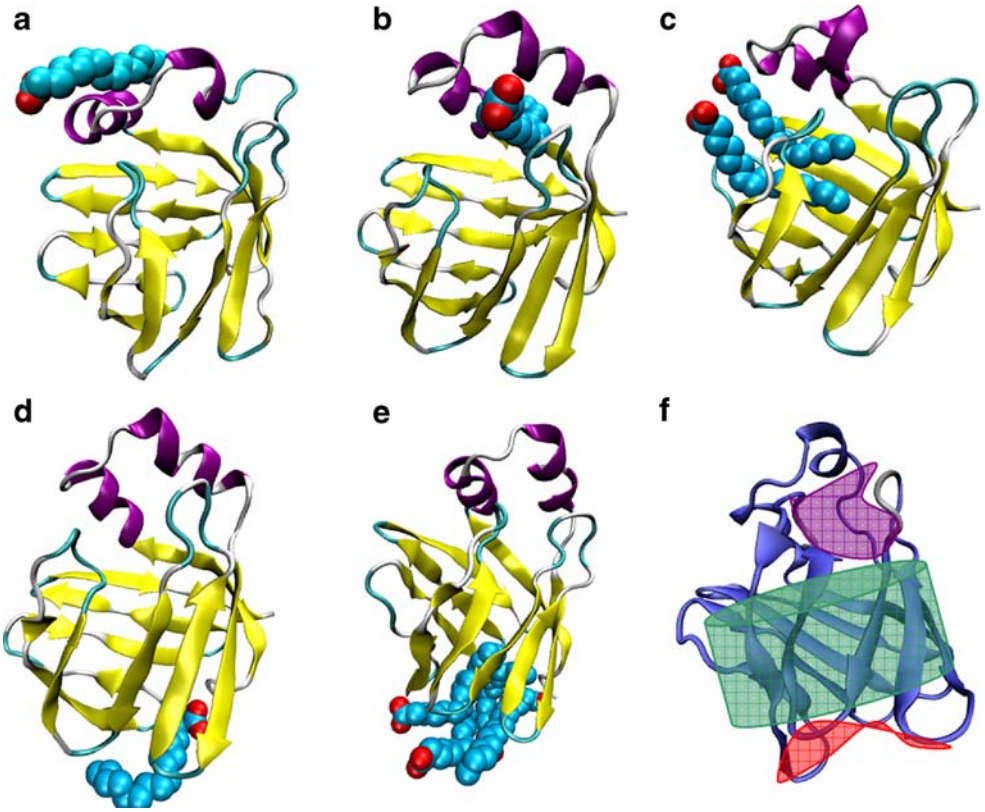

Fig. 2a–f Domains on FABP that interact with PLM ions. **a**–**e** Snapshots representing the major modes of interaction of the protein with the ligand molecules: *violet* helices, *yellow* β strands, *cyan* turns, *white* coils. Note that in some simulations more than one molecule was adsorbed. **e** Mini micelle adsorption. **a**–**c**, **e** Toad Lb-FABP; **d** chicken Lb-FABP. To emphasize the contacts between PLM and the protein, the proteins are not presented in identical orientation. **f** General description of the reactive domains: *violet* main portal, *turquoise* central barrel, *red* anti-portal

rather minor reorientations of the carboxylate moiety with respect to a local positive site on the protein. It should be stressed that the electrostatic interactions are not exclusively with positive residues; for example, the transient burst (~13–17 ns) of electrostatic attraction seen in Fig. 3d is caused by the creation of two hydrogen bonds formed by the PLM with S115; one oxygen atom reacts with the hydroxyl moiety of the serine, while the other oxygen atom of the carboxylate reacts with the backbone NH of the same residue.

In all cases, the LJ and the electrostatic interactions appear to be uncoupled, time wise. In some cases, the initial contact was electrostatic in nature, whereas in others it appears well after adsorption took place. However, the time average contribution of the electrostatic attraction was much smaller than that of the LJ, suggesting that the complex is mostly stabilized by a LJ potential. The value of the LJ attraction is attributed mainly to the reduction of the hydrophobic solvent accessible surface area (SASA). Both values (SASA and LJ) decrease with time although no linear dependence was observed (data not shown). It should be clarified that, at the end of the simulations, the complexes do not represent a final stable complex, but rather a temporary situation leading to the efficient removal of FA from the solution. These temporary complexes may later evolve into more stable structures such as those that appear in the NMR measurements.

It is of interest to point out that, under the experimental conditions used here, the two potentials are effective in a comparable range; the range of electrostatic attraction is effectively shrunk by the screening electrolyte to ~10 Å [at I=50–100 mM the Debye length (κ^{-1}) is ~10–12 Å)]. The LJ potential is operating within a much smaller range, but as the aliphatic chain is some 15–20 Å long, the PLM molecule can establish LJ interactions at a distance comparable to its length, endowing it with an apparent long distance force.

Interaction of the protein with PLM molecules

The electrostatic and LJ interactions of the PLM with the protein are dependent on the proximity of the carboxylate and the aliphatic tails of the FA to the protein. To map the domains where these interactions take place, we summed the locations of all temporal contacts between the various PLM binding domains of the protein with the ligand. This was achieved by scanning all trajectories for snapshots where either the carboxylate, or the aliphatic, tail of the PLM was at a distance of 3 Å (or less) from any heavy atom of the protein (Table 1). These events were further classified by the region of the PLM (carboxylate or aliphatic tail) that was in contact with the protein, and by the protein domain at which the encounter took place. The data are a summation over a wide range of contact

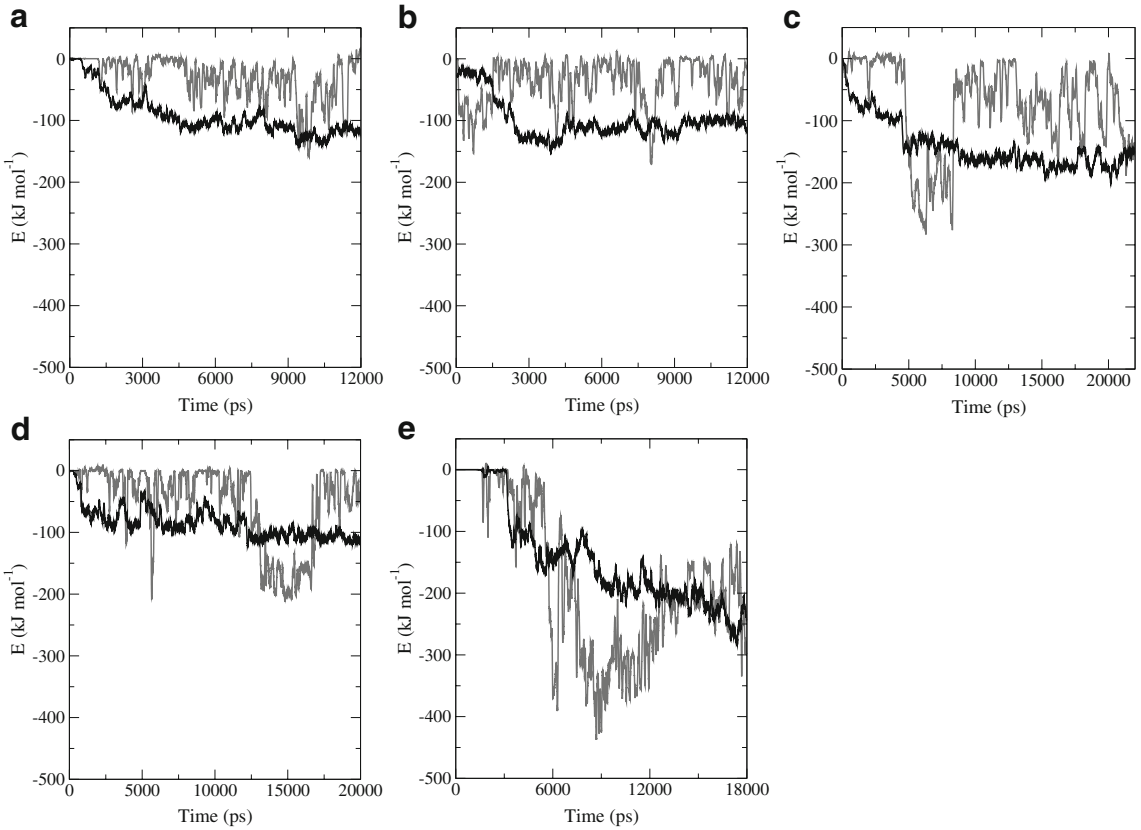

Fig. 3a–e Evolution of the bound state of the PLM ion as a function of time as expressed by the Lennard-Jones (LJ; *black*) and electrostatic (*gray*) potentials calculated for the PLM–protein pair. **a** PLM ion adsorbed to α-helices, as in Fig. 2a; **b**, **c** interaction of ligands with the portal domain (see Fig. 2b,c); **d** interaction of one PLM ion with the anti-portal (Fig. 2d); **e** interaction of FA molecules, already packed in a mini-micelle, with the protein's anti-portal region (Fig. 2e)

stabilities, from brief reversible encounters lasting only few picoseconds, up to those enduring within a nanosecond time frame, i.e., being stable until the end of the simulation time. The brief encounters were found to make a rather small contribution to the accumulated contact time, and for this reason were not excluded from the overall statistics.

The results fall into two main categories. In one, as in runs P6P_III, P6P_VII and TVQ_IV, the PLM molecules spontaneously aggregated into mini-micelle complexes that were stable throughout the entire simulation time. In the other category, the adsorbed PLM ions interacted independently with the protein surface. Both states of the ligand were able to react with the protein. The divergence of the interaction pattern, either at the level of the region of the PLM ion or the domain of the protein to which the FA adsorbed, implies that there is no single preferred mode of interaction.

A contact between the carboxylate moieties and the protein was interpreted as an electrostatically driven interaction whereas the adsorption of the aliphatic tails was a reflection of LJ attraction. As derived from the overall average values (Table 1, bottom row), the two modes of interactions contribute almost equally to the binding. The equivalence of the two energetic terms was also established for each of the simulations even when the bound FA was packed in a mini-micelle, where one could expect LJ interactions to dominate. These interactions were further augmented at the anti-portal domain, where the carboxylate moiety of the FA was found to favor the proximity of charged residues on the β-barrel structure (Table 1, P6P_III and P6P_VII).

Interaction of the PLM molecules with the FABP protein evolved in a repeating pattern even during the relatively short 20 ns simulation time. At the early phase of the simulations, the FA molecules were dispersed randomly in the bathing simulation box. With time, temporary reversible encounters took place, but those where the potential gain was sufficiently high lasted for longer. Finally, through random encounters and relocation of the adhered FA on the protein surface, a well distinguished binding domain could be discerned

Figure 4 provides a comprehensive description of the locations on the PLM molecules with the highest tendency to adhere to the protein, and presents a summation of all contact points (less than 3 Å),between the carboxylate head (Fig. 4a) and the aliphatic tail (Fig. 4b) moieties of the PLM

Table 1 Normalized contacts between the carboxylic head groups and the aliphatic tails of palmitate (PLM) molecules with different regions of toad[a] and chicken[b] liver acid fatty acid binding proteins (Lb-FABPs). For each simulation, the minimal distance between the PLM ions and the specific protein's binding region was calculated. All the frames that showed contact distance shorter than 3 Å were counted. The number of contacts of each run was normalized to 20 ns simulation length. The final values are expressed as a percentage of the local contacts relative to total number of contacts of each simulation. *LJ* Lennard-Jones potential

Type of interaction	Helices outside		Main portal		Central barrel		Anti portal	
	LJ	Electrostatic	LJ	Electrostatic	LJ	Electrostatic	LJ	Electrostatic
P6P_I	3.74	11.14	34.46[d]	49.71[d]	0.35	0.60	0.00	0.00
P6P_II	5.91	24.04[d]	48.79[d]	13.38	6.10	1.77	0.00	0.00
P6P_III[c]	0.00	0.00	0.00	0.00	9.50	29.63[d]	29.31[d]	31.57[d]
P6P_IV	5.85	14.70	21.88[d]	25.80[d]	9.69	13.13	4.87	4.08
P6P_V	2.15	1.64	24.21[d]	30.62[d]	0.26	1.17	16.50	23.45[d]
P6P_VI	9.69	27.20[d]	20.31[d]	33.07[d]	0.29	2.44	4.17	2.84
P6P_VII[c]	0.01	0.01	0.04	0.01	3.06	8.89[d]	38.57[d]	49.40[d]
TVQ_I	1.61	4.47	37.08[d]	18.70	6.43	9.06	10.88	11.77
TVQ_II	0.80	0.41	41.17[d]	32.78[d]	9.20	12.41	1.16	2.08
TVQ_III	4.91	5.45	14.69	8.53	2.27	0.94	35.51[d]	27.70[d]
TVQ_IV[c]	0.00	0.00	0.00	0.00	8.38	8.16	37.03[d]	46.43[d]
Percent of total	3.27	7.97	21.37[d]	21.29[d]	4.35	7.91	15.91	17.93

[a] The different regions of the toad Lb-FABPs are defined as follows: *helices outside* E15, N16, R19, T20, G22, E25, D26, L29, K32, K33; *main portal* Q11, Y14, F17, L18, V21, G22, N23, I27, I28, A31, N35, T53, K55, Q56, H58, S72, M73, N74, K76, K77, I78, D94, K95, I113, G114, S115, S116 R120; *central barrel* N3, G4, T5, N7, Y9, A10, E39, E41, E46, V48, T50, S61, E69, T81, Q83, I90, S97, I99, E101, E106, V108, K110, T112, T119, K121; *anti portal* A1, F2, N3, Q42, G44, N45, F47, V64, G65, L84, G86, G87, G104, D105, V125

[b] The different regions of the chicken Lb-FABPs are defined as follows: *helices outside* E15, E16, K19, A20, A22, P24, E25, D26, K29, M30, R32; *main portal* Q11, Y14, F17, L18, L21, A22, L23, L27, A31, P36, S51, T53, R55, Q56, V58, T71, T72, M73, D74, G75, K76, L78, Y9, A10, E39, Q41, V48, T50, K52, T59, S61, D69, K79, T81, H83, V90, K92, E99, E101, V108, T110, I119, R121; *anti portal* A1, F2, S3, Q42, G44, D45, F47, L64, G65, L84, N86, G87, G104, N105, V125

[c] In these simulations a mini- micelle was observed to react with the protein

[d] Values representing the main contact (above 20%) interaction in each simulation

with the protein. The calculated results were used to mark the protein; thus, the propensity of the different domains to interact with the PLM molecule is color coded from cyan (sporadic encounter) to red (lasting contact). Obviously, major interacting domains are the portal region with the α-helical motif at one side of the protein and the anti-portal domain at the opposite site, while the massive surface area of the β-strands that constitute the β-barrel structure hardly interacts at all with the lipid ligand. These characteristic binding domains do not depend on interaction type; hence, the representations of electrostatic interactions (Fig. 4a) and the picture formed by aliphatic tails (Fig. 4b) are almost identical.

Correlation between domain flexibility and interaction with FA ions

Quantitative analysis of the interaction of the ligand with the FABP structure clearly implicates both portal and anti-portal domains as the preferred domains. The interaction between a protein with a ligand calls for mutual adjustments of structures, i.e., a series of repeated steps of mutual rearrangements of the two reactants, as they optimize their binding energy. Accordingly, we tried to capture these rearrangements and express them by the RMSD of the local domains (Fig. 5). One domain includes the residues of the turns and β-strands around the main portal and the two α-helices covering it, and the other encompassing the residues of the anti-portal and the β-barrel region. The RMSDs of these domains were calculated from MD carried out in presence of ligands and, as a control, for the apo-protein in solution. The results presented in Fig. 5 indicate that, in general, the portal region is significantly more flexible than the anti-portal all over the performed simulations. These results sum 134 ns of the ligand and toad Lb-FABP interactions, and imply that the higher flexibility of the portal domain is an inherent property. This is an unexpected observation as the high value was recorded even in simulations where the binding interactions occurred at the anti-portal domain (P6P_III and P6P_VII).

Comparison of the RMSD values calculated for simulation in the presence of ligand near the protein with those carried out in its absence (inset in Fig. 5) reveals a substantial increase in the fluctuations of protein structure

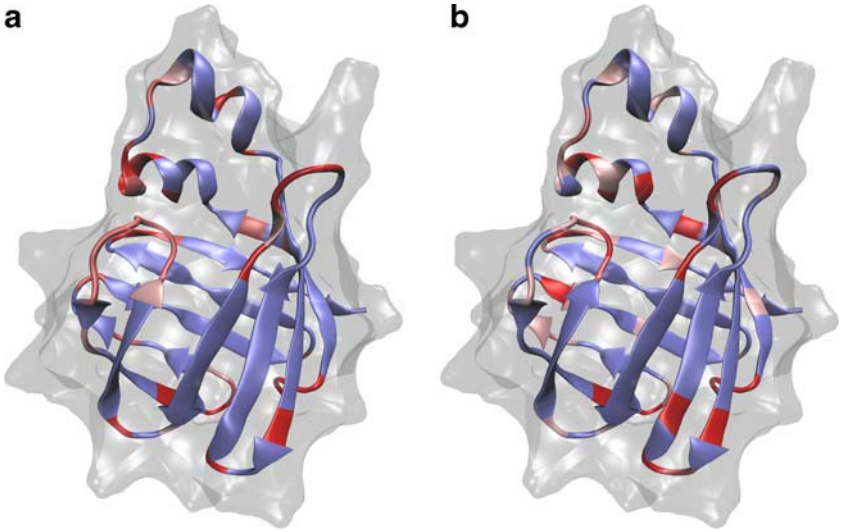

Fig. 4a,b Interacting regions on toad Lb-FABP calculated for 134 ns from seven simulations. The color code refers to the total number of contacts between the carboxyl group (**a**) and the hydrophobic tail (**b**) of the PLM molecule with the protein. A contact is counted when the distance between any atoms of PLM and the protein is less than 3 Å. *Dark red* > 3,000 contacts; *light red* 2,001–3,000 contacts; *pink* 1,000–2,000 contacts; *blue* < 1,000 contacts

at the main portal binding domain, with respect to the values assigned for the Apo-form of the protein. This may reflect the dynamic structural adjustments that must occur in order to form a binding process between the protein and its ligands. These findings are in agreement with the calculated results of Villareal et al. [30], who found conformational changes during binding to the membrane in the portal region even when the interaction of the protein with the membrane was through the anti-portal section of the protein. The inset in Fig. 5 also shows that, on average, the flexibility of the anti-portal area is rather low and is not affected by the binding of ligands, while the higher flexibility of the main portal seems to increase in the presence of PLM molecules.

Concluding remarks

The available crystal structures of FABP-ligand complexes exhibit uniformity in the binding sites. For all crystalline structures, the ligands are fitted snugly inside the inner cavity of the protein with some variation in their orientation depending on the type of the protein (liver, intestinal, etc.) and the nature of the bound compound (FA, cholesterol,

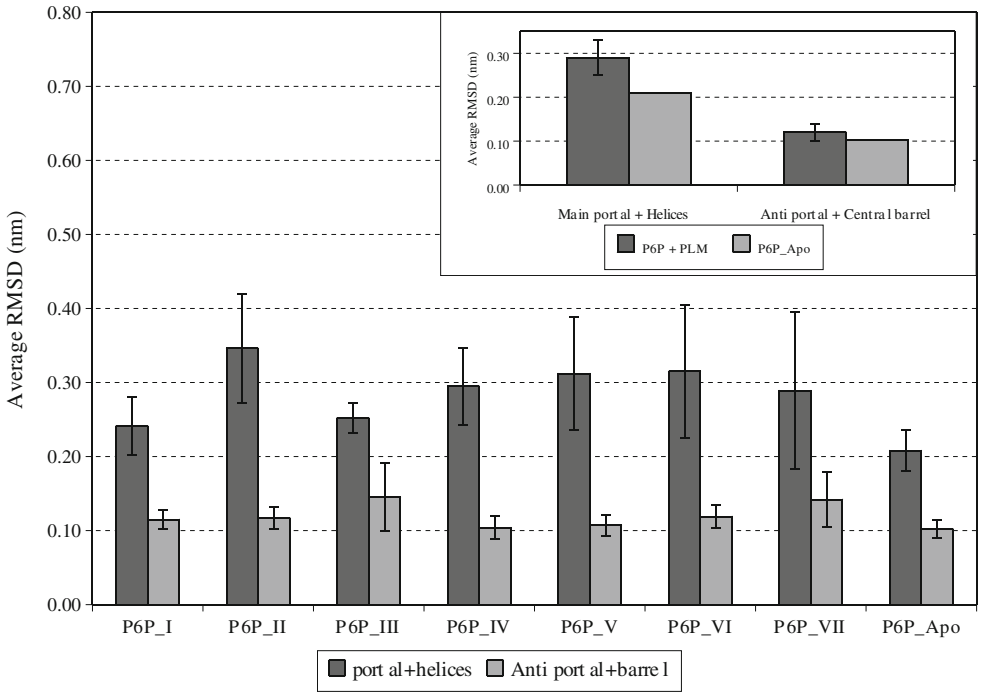

Fig. 5 Averaged RMSD for the 'main portal and α-helices' and for the 'anti-portal and central barrel' regions calculated over the production phase of each simulation. *Inset* Average fluctuations for these regions in the presence (seven simulations) and absence (one simulation) of PLM molecules

bile acid, etc.). In contrast to crystalline protein complexes, which are devoid of internal motion, NMR measurements report signals from a large number of configurations that are in equilibrium with one another [19, 20, 51]. It should be noted that structural data derived by X-ray crystallography are considered essential for clarification of a protein–ligand interaction. However, crystallization is carried out under restrictive conditions that force all molecules to assume the very same configuration. These conditions differ markedly from those prevailing under in vivo conditions, or in vitro NMR experiments.

Other studies also suggest the possibility of more than one primary binding site for FABP. Recent NMR measurements reported by Chuang et al. [20] were performed in a concentrated solution of L-FABP (100 μM) and at various ligand concentrations (20–500 μM). These measurements revealed that different ligands have two binding sites, with high and low affinities, which exhibit a significant H^1–N^{15} chemical shift upon the addition of the ligand. The low affinity binding site is likely to be more promiscuous and capable of interacting with a variety of lipophilic species. The observations of the present simulations are in accord with this NMR study, and the current MD simulations enjoy a time resolution, which is lacking from the NMR measurements. Previously reported MD simulations [23] proposed that the ligand could adsorb to the FABP in more than one location. It was shown that a fatty acid is capable of penetrating deep into the protein from the anti-portal region. These studies imply that, in solution, a ligand and a protein are found in a dynamic equilibrium, and the ligand, through repeated dissociation–association events, samples many sites on the protein. Thus, the formation of a stable complex as envisioned by X-ray analysis is a gradual process having a temporal element that leaves no trace on the final crystalline state of the protein. The interactions detected by the present simulations are those appearing during the numerous initial encounters between the ligands and the proteins. We noted that the ligands were distributed mainly on the portal and anti-portal domains, exhibiting varying levels of penetration into the inner cavity.

According to our results, at physiological ionic strength, where electrostatic interactions tail off at ~10 Å, protein–ligand contacts are initiated by unbiased random encounters. This finally leads to protein–ligand complexes in which either the carboxylate or the aliphatic tail make a long lasting contact. If the initial encounter is at, or near, a site where electrostatic or LJ interactions are permissive, the ligand will strengthen its adsorption to the surface while optimizing the interaction energy. These initial complexes, which represent the earliest phase of holo-protein formation, evolve further on a much longer time scale into complexes with a lifetime long enough to contribute to signals gathered by NMR measurement and, under most favorable conditions (as in crystallization), lead to a singular mode of binding.

Free FA molecules are mild detergents, which at intracellular pH are capable of disrupting the function of cell membrane systems. FABPs, by binding FAs, eliminate the latter from the cytoplasmic matrix. Within the most initial phase of our simulations the FABP proteins exhibited low selectivity and high adsorbing capacity. Thus, by utilizing MD simulations as elaborated in the current study, we were able to track and detect the introductory phases of the elimination process.

Acknowledgments The authors acknowledge the use of computer resources belonging to the Information Technology and Computing Division and to the Bioinformatics Unit at Tel Aviv University.

References

1. Matarese V et al (1989) Intracellular fatty acid trafficking and the role of cytosolic lipid binding proteins. Prog Lipid Res 28(4):245–272
2. Veerkamp JH, Peeters RA, Maatman RG (1991) Structural and functional features of different types of cytoplasmic fatty acid-binding proteins. Biochim Biophys Acta 1081(1):1–24
3. Banaszak L et al (1994) Lipid-binding proteins: a family of fatty acid and retinoid transport proteins. Adv Protein Chem 45:89–151
4. Santome JA et al (1998) Fatty acid-binding proteins. Chronological description and discussion of hypotheses involving their molecular evolution. Comp Biochem Physiol Res Trends 4:23–38
5. Storch J, Corsico B (2008) The emerging functions and mechanisms of mammalian fatty acid-binding proteins. Annu Rev Nutr 28:73–95
6. Di Pietro SM et al (2003) Structural and biochemical characterization of toad liver fatty acid-binding protein. Biochemistry 42 (27):8192–8203
7. Nichesola D et al (2004) Crystal structure of chicken liver basic fatty acid-binding protein complexed with cholic acid. Biochemistry 43(44):14072–14079
8. Zimmerman AW et al (1999) Functional and conformational characterization of new mutants of heart fatty acid-binding protein. Biochem J 344:495–501
9. Zimmerman AW, Veerkamp JH (2002) New insights into the structure and function of fatty acid-binding proteins. Cell Mol Life Sci 59:1096–1116
10. Herr FM, Aronson J, Storch J (1996) Role of portal region lysine residues in electrostatic interactions between heart fatty acid binding protein and phospholipid membranes. Biochemistry 35 (4):1296–1303
11. Ory J et al (1997) Biochemical and crystallographic analyses of a portal mutant of the adipocyte lipid-binding protein. J Biol Chem 272(15):9793–9801
12. Wu F et al (2001) Deletion of the helical motif in the intestinal fatty acid-binding protein reduces its interactions with membrane monolayers: Brewster angle microscopy, IR reflection–absorption spectroscopy, and surface pressure studies. Biochemistry 40(7):1976–1983
13. Jenkins AE et al (2002) Testing of the portal hypothesis: analysis of a V32G, F57G, K58G mutant of the fatty acid binding protein of the murine adipocyte. Biochemistry 41(6):2022–2027
14. Mihajlovic M, Lazaridis T (2007) Modeling fatty acid delivery from intestinal fatty acid binding protein to a membrane. Protein Sci 16(9):2042–2055

15. Corsico B, Liou HL, Storch J (2004) The alpha–helical domain of liver fatty acid binding protein is responsible for the diffusion-mediated transfer of fatty acids to phospholipid membranes. Biochemistry 43(12):3600–3607
16. Likic VA, Prendergast FG (1999) Structure and dynamics of the fatty acid binding cavity in apo rat intestinal fatty acid binding protein. Protein Sci 8(8):1649–1657
17. Hanhoff T, Lucke C, Spener F (2002) Insights into binding of fatty acids by fatty acid binding proteins. Mol Cell Biochem 239 (1–2):45–54
18. Zhang FL et al (2003) Solution structure of human intestinal fatty acid binding protein with a naturally-occurring single amino acid substitution (A54T) that is associated with altered lipid metabolism. Biochemistry 42(24):7339–7347
19. Velkov T et al (2005) An improved method for the purification of rat liver-type fatty acid binding protein from Escherichia coli. Protein Expr Purif 44(1):23–31
20. Chuang S et al (2008) Characterization of the drug binding specificity of rat liver fatty acid binding protein. J Med Chem 51 (13):3755–3764
21. Bakowies D, van Gunsteren WF (2002) Simulations of apo and holo-fatty acid binding protein: structure and dynamics of protein, ligand and internal water. J Mol Biol 315(4):713–736
22. Bakowies D, van Gunsteren WF (2002) Water in protein cavities: a procedure to identify internal water and exchange pathways and application to fatty acid-binding protein. Proteins 47(4):534–545
23. Friedman R, Nachliel E, Gutman M (2005) Molecular dynamics simulations of the adipocyte lipid binding protein reveal a novel entry site for the ligand. Biochemistry 44:4275–4283
24. Friedman R, Nachliel E, Gutman M (2006) Fatty acid binding proteins: same structure but different binding mechanisms? Molecular dynamics simulations of intestinal fatty acid binding protein. Biophys J 90(5):1535–1545
25. Likic VA et al (2000) A "structural" water molecule in the family of fatty acid binding proteins. Protein Sci 9(3):497–504
26. Likic VA, Prendergast FG (2001) Dynamics of internal water in fatty acid binding protein: computer simulations and comparison with experiments. Proteins 43(1):65–72
27. Polverini E et al (2006) The pH-dependent unfolding mechanism of P2 myelin protein: an experimental and computational study. J Struct Biol 153(3):253–263
28. Rich MR, Evans JS (1996) Molecular dynamics simulations of adipocyte lipid-binding protein: effect of electrostatics and acyl chain unsaturation. Biochemistry 35(5):1506–1515
29. Tsfadia Y et al (2007) Molecular dynamics simulations of palmitate entry into the hydrophobic pocket of the fatty acid binding protein. FEBS Lett 581(6):1243–1247
30. Villarreal MA et al (2008) Binding and interactions of L-BABP to lipid membranes studied by molecular dynamic simulations. Biochim Biophys Acta 1778(6):1390–1397
31. Wagoner J, Baker NA (2004) Solvation forces on biomolecular structures: a comparison of explicit solvent and Poisson-Boltzmann models. J Comput Chem 25(13):1623–1629
32. Woolf TB (1998) Simulations of fatty acid-binding proteins suggest sites important for function. I. Stearic acid. Biophys J 74:681–693
33. Woolf TB, Grossfield A, Tychko M (2000) Differences between apo and three holo forms of the intestinal fatty acid binding protein seen by molecular dynamics computer calculations. Biophys J 78(2):608–625
34. Woolf TB, Tychko M (1998) Simulations of fatty acid-binding proteins. II. Sites for discrimination of monounsaturated ligands. Biophys J 74(2):694–707
35. Zanotti G, Feltre L, Spadon P (1994) A possible route for the release of fatty acid from fatty acid-binding protein. Biochem J 301(Pt 2):459–463
36. Zou H et al (2007) Molecular insight into the interaction between IFABP and PA by using MM-PBSA and alanine scanning methods. J Phys Chem B 111(30):9104–9113
37. Levin LB et al (2009) Molecular dynamics study of the interaction between fatty acid binding proteins with palmitate mini-micelles. Mol Cell Biochem 326(1–2):29–33
38. Moran JB et al (1987) Protein binding of palmitate measured by transmembrane diffusion through polyethylene. Anal Biochem 167(2):394–399
39. Berendsen HJC, van der Spoel D, van Drunen R (1995) GROMACS: a message-passing parallel molecular dynamics implementation. Comp Phys Commun 91:43–56
40. Lindahl E, Hess B, van der Spoel D (2001) Gromacs 3.0: a package for molecular simulation and trajectory analysis. J Mol Model 7:306–317
41. van Der Spoel D et al (2004) Groningen machine for molecular simulations. BIOSON Research Institute, Groningen
42. Oostenbrink C et al (2004) A biomolecular force field based on the free enthalpy of hydration and solvation: the GROMOS force-field parameter sets 53A5 and 53A6. J Comput Chem 25(13):1656–1676
43. Berman HM et al (2000) The protein data bank. Nucleic Acids Res 28(1):235–242
44. Schuttelkopf AW, van Aalten DM (2004) PRODRG: a tool for high-throughput crystallography of protein–ligand complexes. Acta Crystallogr D Biol Crystallogr 60(Pt 8):1355–1363
45. Berendsen HJC et al (1969) Interaction models for water in relation to protein hydration. Nature 224:175–177
46. Hess B et al (1997) LINCS: a linear constraint solver for molecular simulations. J Comp Chem 18:1463–1472
47. Miyamoto S, Kollman PA (1992) SETTLE: an analytical version of the SHAKE and RATTLE algorithms for rigid water models. J Comp Chem 13:952–962
48. Berendsen HJC et al (1984) Molecular dynamics with coupling to an external bath. J Chem Phys 81:3684–3690
49. Essman U et al (1995) A smooth particle mesh Ewald method. J Chem Phys 103:8577–8592
50. Humphrey W, Dalke A, Schulten K (1996) VMD: visual molecular dynamics. J Mol Graph 14(1):27–28, 33–38
51. Ogbay B, Dekoster GT, Cistola DP (2004) The NMR structure of a stable and compact all-beta-sheet variant of intestinal fatty acid-binding protein. Protein Sci 13(5):1227–1237